Acta Materialia 209 (2021) 116786

Contents lists available at ScienceDirect

Acta Materialia

journal homepage: www.elsevier.com/locate/actamat

Grain boundary phase transformation in a CrCoNi complex concentrated alloy

Fuhua Cao[a,c], Yan Chen[a,c], Shiteng Zhao[d], En Ma[a], Lanhong Dai[a,b,c,*]

[a] State Key Laboratory of Nonlinear Mechanics, Institute of Mechanics, Chinese Academy of Sciences, Beijing 100190, PR China
[b] State Key Laboratory of Explosion Science and Technology, Beijing Institute of Technology, Beijing, 100081, China
[c] School of Engineering Science, University of Chinese Academy of Sciences, Beijing 101408, PR China
[d] Department of Materials Science and Engineering, University of California, Berkeley, CA, USA

ARTICLE INFO

Article history:
Received 4 December 2020
Revised 24 February 2021
Accepted 25 February 2021
Available online 2 March 2021

Keywords:
Grain boundary
Structural transformation
Medium-entropy alloy
Local chemical order
Diffusion

ABSTRACT

The phase-transformation-like behavior of grain boundaries, where their chemistry, structure and properties change discontinuously, is emerging as a fundamental interest in the context of grain boundary engineering. The cases studied so far pertain primarily to elemental metals and dilute alloy systems. The next step of complexity would be a system still of a single phase structure but involving multiple and concentrated elements. The recently emerging high/medium entropy alloys (H/MEAs), alternatively known as complex concentration alloys (CCAs), fit the bill in this regard. Here we use CoCrNi as a model CCA to highlight that intricate interatomic interactions influence the grain boundary element distribution and consequently phase transitions. By combining classical molecular dynamics simulations and first-principles density functional theory calculations, we reveal that grain boundary phase transition temperature is sensitive to the grain boundary atomic configuration. The CCA grain boundary with random atomic distribution is more apt to transform due to a larger thermodynamic driving force and faster diffusion kinetics, compared to a hypothetical reference that bears the same bulk properties but no distinguishable constituent components. In contrast, when the three elements redistribute with local Ni-clustering and Co–Cr ordering in the grain boundary structure, diffusion is rendered more sluggish, delaying grain boundary phase transformation. Our work is a step forward in understanding critical phenomena in grain boundaries and CCAs, and enriches the knowledge base for materials design via grain boundary engineering.

1. Introduction

Grain boundaries (GBs) are essential defects for polycrystalline materials, playing a key role in mechanical, thermal, electrical and many other material properties [1–6]. Recent years have seen a rapid growth of evidence suggesting that the change of GB properties can occur via a GB phase transition (also called GB "complexion" transition) that leads to abrupt changes in GB structure and chemistry, which in turn drastically alters various GB-sensitive material properties, such as grain growth, activated sintering, ductility and creep [7–16]. Thermodynamically, the GB complexion transition occurs when there is a discontinuity in the first or higher-order derivative of GB energy as a function of thermodynamic parameters such as temperature, pressure, and chemical potential [7,17,18]. These transitions typically occur independently of bulk phase transformations and can be triggered in several ways by varying the temperature [18], pressure [9], atomic density [19,20], and element segregation [21,22]. Among these, the role of element segregation on GB phase transformations received special attention [12,22,23], since it is a common phenomenon in most alloys that is routinely used in alloy design [2,24,25]. It has been suggested that the GB phase transitions are affected by the attractive or repulsive interactions and site competition among different elements that change the GB structurally and thermodynamically [7,22,23,26,27].

However, these studies have focused primarily on dilute binary systems, in which segregation induced structural and energy disturbance is limited. Little is known about the GB phase transition behavior in the recently emerging complex concentration alloys (CCAs) or high/medium entropy alloys (H/MEAs) with multi-principal elements at high concentrations, in which the presence and interaction of multiple components in GB may produce novel physical phenomena that are unattainable otherwise. For example, the FeMnNiCoCr CCA was reported to show heterogeneous

* Corresponding author at: State Key Laboratory of Nonlinear Mechanics, Institute of Mechanics, Chinese Academy of Sciences (CAS), Beisihuanxi Road, No. 15, Beijing 100190, China.
E-mail address: lhdai@lnm.imech.ac.cn (L. Dai).

https://doi.org/10.1016/j.actamat.2021.116786
1359-6454/

segregation of three principal elements in GB, in which Ni and Mn co-segregate to some GB regions while Cr is enriched in other regions [28]. This nano-clustering of multi- principal elements further reduces GB cohesion and promotes crack initiation along GBs that leads to a ductility loss [29]. Similar rapid decrease in ductility at intermediate test temperatures (400° to 800 °C) was also found in other CrCoNi-based CCAs [29]. These rapid nano-clustering during deformation may be associated with the substantial change in the GB diffusion properties at intermediate temperatures. For example, it has been shown that the CoCrFeNi alloy suffered remarkable grain growth at 800 °C, suggesting an abrupt change of GB diffusion properties at this temperature [30]. Recently, Rajeshwari et al. [31] found the GB diffusivities can be changed through heat treatment and demonstrated the existence of GB phase transitions in Ni–Cr–Fe alloy. These results suggest that there may also exist a discontinuous GB structure or chemistry transition that markedly alter GB properties at intermediate temperatures in CCAs.

The atoms in CCAs occupy crystallographic lattice sites with a high degree of chemical disorder [32–39]. However, the multi-principal elements are potentially subject to complex interactions in bulk and especially in GB, beyond what is expected for a random solid solution (RSS). Besides, CCAs are recognized as an exciting new class of metallic structural materials due to their attractive mechanical properties in conventional [39–45] and harsh environments [46–48]. Therefore, the prediction and characterization of segregation behaviors and their effect on GB complexion transitions in CCAs are of much practical and fundamental interest. The interaction of multiple elements in CCAs makes the GB element distribution and structural transition pathway more difficult to track, due to the rugged atomic and energy landscape in bulk and GB [23,25]. Analogous to composition inhomogeneity in the bulk [49–52], the heterogeneous segregation or clustering of principal elements at GBs reported recently can be considered as a manifestation of local chemical order (LCO) in GBs [28,29], which may further affect GB composition [24] and structural transition behavior. It is thus of interest to explore how the intricate interactions among principal elements in a concentrated solution affect the GB structural transition behaviors in CCAs, in a way different from traditional metals and dilute systems.

To explore this issue, we choose to start with CrCoNi as the first model CCA. Incidentally, this CCA is a prototypical H/MEA that exhibits an excellent combination of mechanical properties including good strength, large ductility, and high fracture toughness at ambient-to-cryogenic temperatures [42,53–57]. In terms of modeling GB transformation, this medium-entropy alloy CrCoNi satisfies our needs; it is a concentrated alloy beyond the simple metals or dilute solutions already studied. Yet, this CCA is still a single fcc phase, with only three elements that are not very different in atomic size and have only small heat of mixing. The atomic strain and local chemical ordering is therefore expected to be only moderate. As such, CrCoNi represents the next level of complexity, one that is a step beyond elemental metals or dilute solutions (e.g., ideal solution), but can still be close to a random solution or a solution with only moderate degree of local chemical order, far less complicated than CCAs with even more elements, severe lattice distortion or the potential to precipitate out a second phase.

Direct experimental observations of complexion transitions are extremely difficult, especially for the CCAs that exhibit atomic mismatch and chemical fluctuations [8,58,59]. Atomistic computer simulations have proven to be an invaluable tool for the study of GBs, in providing atomic-scale details of the evolution of GB structures [9,12,15,19,20,60–63]. We therefore resort to molecular dynamics (MD simulations) coupled with first-principles DFT calculations in this work, to elucidate the elemental distribution at the atomic level in GBs and the GB transition in the CrCoNi model CCA.

2. Methods

2.1. MD simulations

MD simulations were performed using the Large-scale Atomic/Molecular Massively Parallel Simulator (LAMMPS) package [64] with recently developed DFT-calibrated embedded-atom potential for CrCoNi CCAs by Li et al. [49]. To help distinguish the GB structural transformation behaviors of CCA for elemental metals, calculations are repeated on a derived hypothetical pure average-atom interatomic potential, which bears the same bulk properties of equi-atomic CrCoNi CCA but no lattice distortion and LCO [65]. The symmetrical tilt Σ5 (210) GBs (STGB) was chosen as the main model system in this study because it is a representative high-angle GB for fcc metals and importantly it exhibits a structural transformation at relatively low temperature in other fcc metals [9,20,66]. A bi-crystal model containing two identical Σ5 (210) symmetrical tilt GBs separated by a sufficient thickness (~7.9 nm) of one grain lattice in between was created by joining two crystals rotated relative to each other around the [001] direction by the angle of 53.13°.

To create the random solid solution (RSS) GB configuration, the Ni atoms in the original GB model were randomly selected and replaced with Co and Cr until the equal molar ratio was achieved. Segregation in the GB is simulated using a Monte-Carlo (MC) algorithm in the variance-constrained semi-grand-canoncial (VC-SGC) ensemble [67]. The hybrid MC/MD simulations are performed to ensure that the systems are relaxed simultaneously in both chemical and structural freedom. The parameters of $\Delta\mu_{\mathrm{Ni-Co}} = 0.021$ eV and $\Delta\mu_{\mathrm{Ni-Cr}} = -0.31$ eV are set to achieve an equi-atomic concentration [49]. This chemical potential differences were fixed in these MCMD simulations at different temperatures, which is conventional in hybrid MC/MD method [49,61]. During the MC/MD simulation, the 1 MC steps were performed on 1/4 of the atoms every 20 MD steps with timestep of 2.5 fs. The simulations are performed at different annealing temperatures in the NPT ensemble under zero pressure. We also perform pure MC simulations to only consider the chemical effect on element portion, by setting 1MD step every MC cycle and not defining an integration fix such as NPT or NVT.

The constructed bi-crystal models were all first thoroughly relaxed with energy minimization and then equilibrated in isobaric-isothermal (NPT) ensemble under zero pressure. To model the GB transformation, we performed independent isothermal simulations at temperatures varying from 100 K to 1400 K with the increment of 100 K. To study the effect of vacancy on the GB transition, the atoms within the GBs were removed randomly with the fraction of 1%, 3% and 5%, respectively. Periodic boundary conditions were applied along all three directions in all the simulations to exclude all sources/sinks of atoms other than the GB that would cloud the effect of vacancies, by considering the fact that a supply of atoms was not necessary to achieve the transformation [8,20]. Each isothermal simulations were performed in the NPT ensemble with Nose–Hoover thermostat for 10 ns which was sufficient for a phase transition [20].

Prior to diffusion calculations, the blocks were thermally equilibrated for 100 ps at each specific targeted temperature by using a Nose-Hoover thermostat within an NPT ensemble. Then a “diffusion anneal” simulation is performed for each model for 1 to 10 ns, depending on the temperature, which allows us to reach the effective diffusion coefficient [63]. The diffusivities are determined by linearizing a plot of mean-squared displacement (MSD) versus time after 500 ps, where a linear relation has been well established. To investigate the diffusion in the GB core, the MSDs are averaged from the atoms within a window of ±0.3 nm around GB.

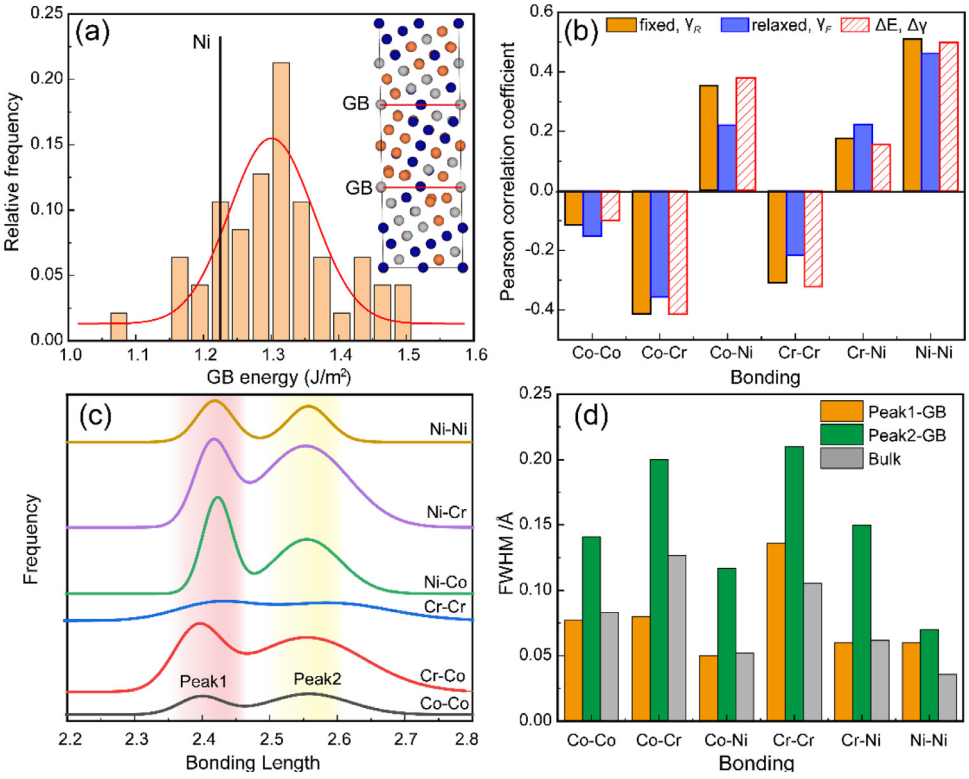

Fig. 1. Energy and atomic structure distribution of Σ5 (210) STGB calculated by DFT: (a) The distribution of the GB energy (b) Correlation between chemical bonding and GB energy (c) bonding length distribution in GBs (d) The full width at half maximum (FWHM) of the bonding length peak in GB and bulk.

All atomic configurations were visualized using the Ovito package [68].

2.2. First-principles calculations

To further study the mechanisms underlying the element segregation and vacancy formation and migration in the Σ5(210) GB, DFT based energy calculation was carried out using a plane wave method, as implemented in the Vienna Ab initio Simulation Package (VASP) [69]. A category of quasi random (210) surface supercell structures with *x*, *y*, and *z* along [001] [−120] and [210] crystal orientations, respectively, were generated through a Monte Carlo (MC) algorithm using the Alloy Theoretic Automated Toolkit (ATAT) package developed by Alex van de Walle et al. [70]. The atoms within $z =$ 0.25 to 0.75 of these random (210) surface supercells were transformed symmetrically to create the sandwich Σ5 (210) STGB supercells [71], as shown in the inset in Fig. 1a.

Eighty independent (210) surface and corresponding GB supercells are calculated to obtain the GB formation energy by

$$\gamma = \frac{1}{2S}\left(E_{GB} - E_{surf}\right) \quad (1)$$

where S is the area of the GB, E_{GB} and E_{surf} are the total energies of the sandwich GB supercell and the corresponding surface supercell, respectively. For GB vacancy calculations, a single vacancy was introduced to the fully relaxed GBs by simply removing one atom form a preselected site, followed by a full relaxation for energy minimization. 72 different vacancy sites within a window of ±4 atomic layers around the GB plane (red lines in the GB structure shown in Fig. 1a) were in turn calculated for 5 random selected GB structures. The GB vacancy formation energy is given by

$$E_f = E_v - E_0 + \mu_v \quad (2)$$

where E_v and E_0 are the total energy of the GB supercell with and without the vacancy, respectively, and μ_v is the chemical potential of the vacancy species which is calculated following the method described in Ref. [72]. The Climbing Image Nudged Elastic Band (CI-NEB) method [73] is used to determine the activation energy barriers for the vacancy diffusion by considering several different diffusion paths.

A gradient-corrected functional in the Perdew–Burke–Ernzerhof (PBE) form was used to describe the exchange and correlation inter-actions in DFT [74]. Electron-ion interactions were treated within the projector-augmented-wave (PAW) method [75]. A sufficiently high energy cutoff of 380 eV was adopted for the plane-wave basis set expansion. The energy convergence criterion was set to be 10^{-6} eV in the self-consistent iteration loop and the force criterion on each atom was set to be within 0.02 eV/Å. Brillouin zone integrations were performed using 3 × 3 × 1 Monkhorst-Pack k-point grids. Collinear spin polarization (ISPIN = 2) is enabled in all the calculations.

3. Results and discussions

3.1. GB structure and energy

Fig. 1a shows a wide range of GB energy for the Σ5 (210) STGB with random atomic configuration, which is in contrast to a single value for a pure or perfectly ordered crystalline alloy. As seen, the GB energies obey the Gaussian distribution with a mean value of ~1.3 J/m^2, which can be compared with corresponding GB energy of pure Ni (~1.23 J/m^2, black line in Fig. 1a). Fig. 1b shows the Pearson correlation coefficient between the GB energy and the pairwise LCO parameter. Both the energy calculated with and without atom relaxation (labeled as relaxed and fixed respectively) as well as their difference ($\Delta\gamma$) are analyzed to decouple the chemical effect and structure effect. Specifically, the fixed GB energy (γ_F) is rooted

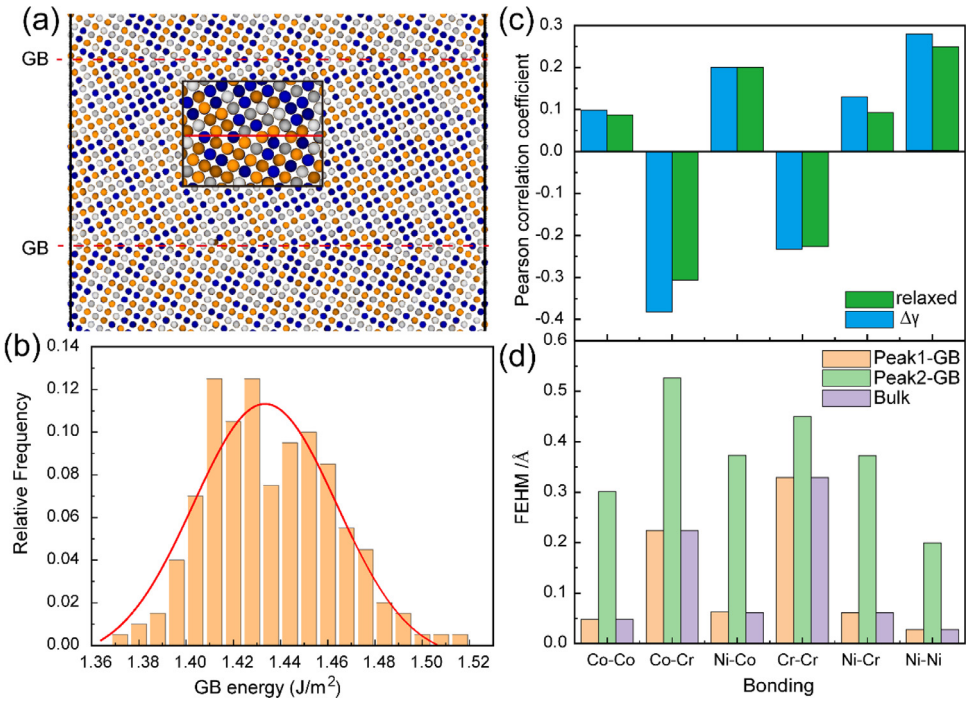

Fig. 2. Energy and atomic structure distribution of Σ5 (210) STGB calculated by MD: (a) The Σ5 (210) STGB atomic structure mode for MD simulation (b) The distribution of the GB energy (c) Correlation between chemical bonding and GB energy (d) The full width at half maximum (FWHM) of the bonding length peak in GB and bulk.

in the chemical effect and $\Delta\gamma$ is related to the structural effect. Both the relaxed and fixed GB energy (γ_R and γ_F) show moderate positive correlation (>0.4) with the order parameter of Ni–Ni and negative correlations (<−0.4) with Co–Cr, suggesting that the GB energy increases with the number of Ni–Ni pair while decreasing with the number of Co–Cr pair. Interestingly, the energy reduction ($\Delta\gamma$) caused by structure relaxation is also proportional to Ni–Ni pair and inversely linked to Co–Cr pair, implying that the increase in Ni–Ni pair can decrease the GB energy, and Co–Cr does the opposite. This seems to contradict the result that the GB energy increase (decrease) with the number of Ni–Ni (Co–Cr) pairs. A plausible explanation for this puzzling result is that the increasing (decreasing) Ni–Ni (Co–Cr) pair can increase the GB energy by its chemical effect while it can also decrease the energy from the structural standpoint. The same sign (positive/negative) of correlation coefficient of γ_F and $\Delta\gamma$ proved that the GB energy is the consequence of a competition between chemical and structure effects.

To further understand the correlation between atomic pairs and structure effect, we calculated the bonding length distribution within the GB region based on ~1500 evaluated bonds for each pair, the results are shown in Fig. 1c. There are two obvious peaks for all the pairs except Cr–Cr, corresponding to the first and second nearest-neighbor atoms within the GB region, respectively. Note that the average bond length and distribution width are varying with the pairs, suggests apparent interatomic bond distortion. To assess the magnitude of these distortions, we have measured the full width at half maximum (FWHM) of the bond length distribution (within 3 Å) within the GB (see Fig. 1c) and bulk region, the results are shown in Fig. 1d. Overall, the FWHM of various pairs show the same trend in GB and bulk region. Among these, the Ni–Ni pair possess the minimum FWHM suggesting a minimum structure distortion. This may result from the delocalized electronic behavior of Ni, which causes a small variation in the bond length. On the contrary, Cr shows an obvious localized electronic behavior which exhibits weak bonding ability and causes a large variation in bond length [76], as manifested by the large fluctuations of Cr–Cr bond lengths. A comparison of Fig. 1b and d reveals that the atom pairs with small distortion often play a positive role in the energy reduction by decreasing the strain energy. The obvious examples are Ni–Ni and Co–Ni pairs which exhibit moderate positive correlation with the relaxation induced energy reduction ($\Delta\gamma$).

We repeated the same analysis shown in Figure 1 by using the interatomic potential. As shown in Fig. 2b, the GB energies also obey the Gaussian distribution with a mean value of ~1.43 J/m^2, which is comparable with that calculated by DFT. Note that the relaxed and difference ($\Delta\gamma$) GB energies show a weaker positive correlation (~0.3) with the order parameter of Ni–Ni than the DFT results (>0.4). This difference may be due to the magnetic effects which would affect the magnitude of order parameters [49]. Nevertheless, the correlation coefficient of Ni–Ni pair with GB energy is the largest other than Co–Cr pair, suggesting a non-negligible effect in GB energies of Ni–Ni pair. The EAM model also captures the moderate negative correlations of Co–Cr pair with GB energies, which is consistent well with the DFT results. In addition, comparison of Fig. 2c and d also reveals the positive role of small distortion in the GB energy reduction. In conclusion, the predictions about chemical ordering and GB energetics calculated by MD are in good agreement with that of DFT, suggesting that the employed interatomic potential can effectively describe the grain boundary behaviors including energy, structure and element distribution.

Recall that both γ_R and γ_F have positive correlation with the Ni–Ni pair and negative correlations with Co–Cr. It seems to indicate a preference for Co–Cr, while disfavoring Ni–Ni pairs in this GB. Note that the results are calculated at 0 K where the structure effect is limited. When the structure becomes dominant at higher temperatures, more Ni–Ni pairs are favorable, to reduce the distortion induced energy. To verify this conjecture, we used MC/MD simulations to investigate whether the mentioned structural effect of Ni–Ni and Co–Cr pairs persist or even magnify at higher temperatures where thermally induced structure distortion prevails. As shown in Fig. 3a, the hybrid MC/MD method that includes both chemical and structural effects leads to pronounced segregation of Ni above 200 K, suggesting a strong segregation trend of Ni.

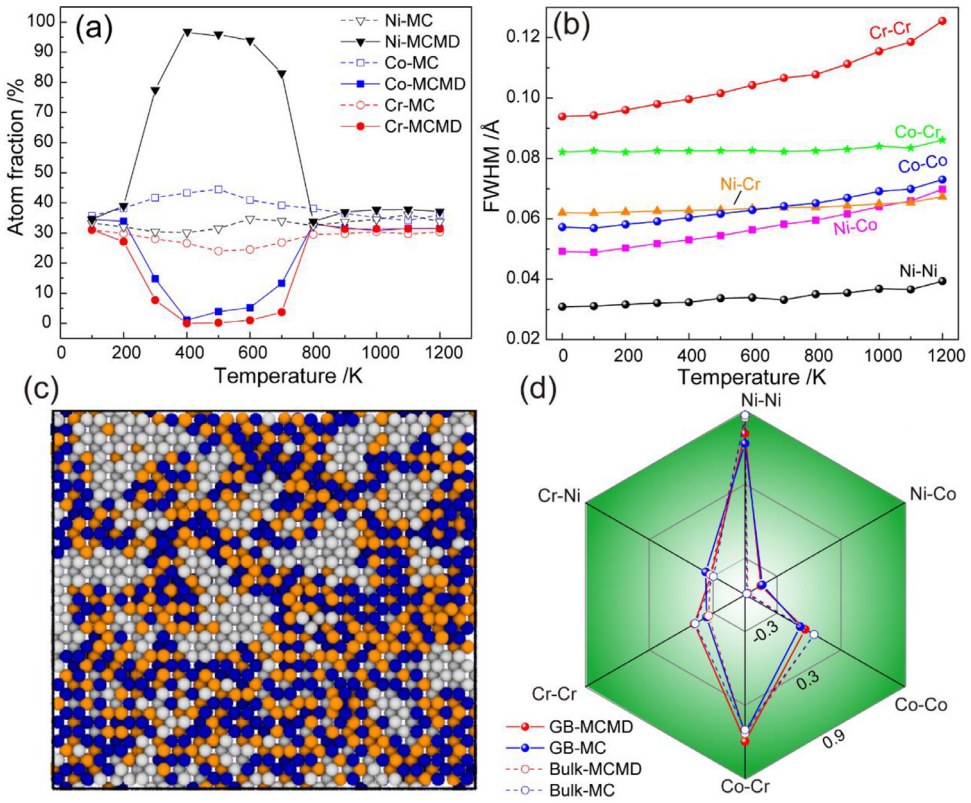

Fig. 3. Partition of Ni (gray), Co (blue) and Cr (orange) in Σ5 (210) STGB: (a) element fraction in GB as a function of MC/MD simulation temperature (b) The FWHM of the bonding lengths as a function of temperature (c) top view of GB structure for annealed GB configuration obtained by MC/MD simulating at 100 K (d) The local order parameter of chemical pairs in the random and 100 K annealed configuration in GB and bulk region.(For interpretation of the references to color in this figure legend, the reader is referred to the web version of this article.)

For pure MC simulations that only reflect the chemical effect, the composition fluctuation is much more moderate than that of hybrid MC/MD simulation, suggesting that the chemical effect is less sensitive to temperature. Nonetheless, the atomic fraction of Co is slightly higher than Ni and Cr, implying that Co is favored to segregate to GB from the chemical energy perspective.

Comparing the segregation behaviors simulated by hybrid MC/MD and pure MC method indicates the decisive role of structural effect in GB segregation at intermediate temperatures. Specially, the structure effect leads to conspicuous Ni segregation at intermediate temperatures. This is in accordance with the recent experimental result that Ni content in GB monotonically increases over time with aging time at 450 °C (723 K) in a NiCoCrMnFe HEA [28]. This thermally governed GB segregation process may be related to thermal enhanced structural distortion. As shown in Fig. 3b, the FWHM of Ni–Ni pair is the lowest and not sensitive to temperature, suggesting a negligible structural distortion even at elevated temperatures. Instead, the FWHM of the Cr–Cr pair is much larger than others that continuously increase with temperature, leading to a considerable distortion especially at high temperatures. Therefore, the segregation of Ni and anti-segregation of Cr in this GB is favorable for stabilizing the GB. Interestingly, the content of Ni decreased rapidly at 600 K before it returns to an average value of ~ 37% at 800 K. This would be ascribed to the structural transformation to be discussed later.

Fig. 3c exhibits the top view of GB atomic distribution after hybrid MC/MD simulation at 100 K, where the atoms are in near equal molar ratio. Remarkably the Ni atoms are clustered while Co and Cr atoms are mutually dissolved. Fig. 3d shows the local chemical order parameter (α_{ij}, i, j are Ni, Co or Cr) of each pairs in GB and bulk region after hybrid MCMD simulation at 100 K, along with corresponding MC simulated values. As seen, the most pronounced local chemical ordering are Ni–Ni and Co–Cr pairs in both hybrid MC/MD and pure MC simulation, which indicates a strong preference for Ni–Ni and Co–Cr pairs in this scenario. One may note that the α_{Ni-Ni} value in bulk is slightly higher than in GB for both MC and hybrid MC.MD simulation, implying an anti-clustering trend for Ni–Ni in GB. This result is in accordance with the DFT-based energy analysis that GB energy is increased with Ni–Ni pairs at 0 K. Comparison of the hybrid MC/MD to the pure MC sample allows for a direct assessment of the effect of structure distortion on the ordering. Careful observation reveals that the value of α_{Ni-Ni} is higher in hybrid MCMD simulation than in pure MC simulation in GB. However, the exact opposite was observed in the bulk. This implies that the structure distortion in GB facilitates the clustering of Ni–Ni, which also conforms to the DFT-based result that increasing Ni–Ni pair leads to more relaxation induced energy reduction ($\Delta\gamma$). All of these suggest a clustering and segregation trend of Ni caused by structure distortion in GB.

3.2. GB structure transformation

In the next step, we used MD simulations to investigate the GB transition in CCA and how the LCO affects the GB complexion transition. Fig. 4a–c show the structure evolution of the Σ5 (210) STGB for the hypothetical pure element average-atom (NiCoCr-Averaged), random (NiCoCr-Random) and Ni-clustered (NiCoCr-Clustered) GB configuration, respectively. For Ni-clustered GB configuration, we select the structure obtained by hybrid MC/MD simulation at 100 K (see Fig. 3c), where the atoms are in near equal molar ratio. Obviously, at low temperatures all of these GBs consist of a series of 'Normal Kite' structure units just like other fcc metals [20,71].

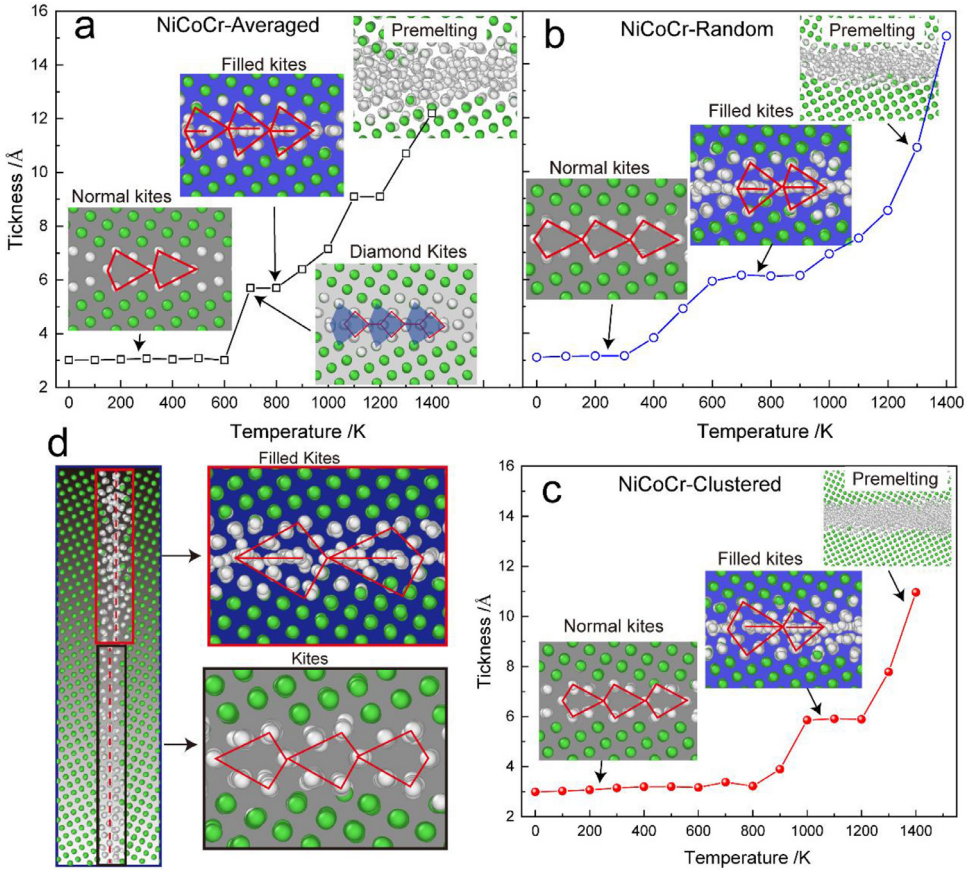

Fig. 4. GB evolution as function of temperature: (a) NiCoCr-Averaged GB (b) NiCoCr-Random GB (c) NiCoCr-Clustered GB (d) The boundary undergoes a first-order phase transformation in NiCoCr-Random GB at 500 K.

They then transform into Filled Kite structure following a significant reduction in thickness to a stable value until further transformation. This transformation behavior has been found in other fcc metals [9,20,66] and verified here for CCAs, suggesting that it represents a generic feature of Σ5 (210) STGB in FCC metals. Different from the other two NiCoCr GBs, the hypothetical pure NiCoCr-Averaged GB possess a Diamond Kites structure before Filled Kite structure, which is consistent with what was reported in pure Cu [9]. As seen in Fig. 4a, the Diamond Kites structure is much similar to the Filled Kite, and can be considered as the Filled Kite with less disturbance. The absence of this Diamond Kites structure in the other two NiCoCr GBs suggests more disturbance in CCA GBs during structural transformation, owning to their complex multiple elements interaction. Note that the transformation form Kites structure to Diamond/Fill Kites is abrupt in hypothetical pure element NiCoCr-Averaged GB and NiCoCr-Clustered GB, while it proceeds in a gradual manner for the NiCoCr-Random GB. The severe disorder and distortion may be responsible for this early but slow transition in the NiCoCr-Random GB.

Fig. 4d demonstrates that the Kites and Fill Kites structures can coexist in NiCoCr-Random GB, in which they are separated by a line defect with a faulting of the GB plane (dash line). Similar two-phase coexistence is also found in NiCoCr-Clustered GBs. These lead us to consider kinetically the GB diffusion as a critical factor controlling phase transformation. Further increase in temperature resulted in a disorder structure and eventually pre-melting near the melt point. Unlike that reported for pure Cu [9,20], we were unable to find the split kites structure in the hypothetical pure NiCoCr-Averaged and the other two NiCoCr GBs, even though the simulation temperature was as high as 1400 K. For additional verification, simulations were repeated with different boundary conditions in the *x* direction, but only Kites and Filled Kite structures were invariably found.

To understand this phase transformation behavior in more detail, we assessed the variation of GB excess free energy, GB entropy and GB excess atomic volume (EFV) as a function of temperature. The free energy calculations were performed using nonequilibrium simulation methods following the methodology in Ref. [77], and the results are shown in Fig. 5a. As expected, all of considered GBs experience a significant decrease in free energy during phase transformation. The large reduction in free energy induced by phase transition suggests that the Fill-Kite structure is more stable than the Kite structure at high temperatures. Specially, the free energy difference in NiCoCr-Random GB is the largest, suggesting the largest energetic driving force for GB phase transformation. Generally, the free energy of GB with a consistent composition is expected to decrease linearly with increasing temperature because of the entropic term in the free energy [78–80]. Although Fig. 5a shows discontinues changes in GB free energy that happen far away from the two phase equilibrium coexistence temperature, it does not mean that the phase transformations begin above the equilibrium coexistence temperature. The GB structure shown in Fig. 4d demonstrates that the Kites and Fill Kites structures can coexist during transformation, which is similar to the GB phase transformation behavior found in element Cu [81]. This suggests that GB phase transformations occur within the equilibrium coexistence temperature [7]. A close comparison of Figs. 5a and 4a–c reveals that the abrupt changes in GB free energy appear at temperatures higher than the phase transition point as marked by the arrows in Fig. 5a. At these transition initiation temperatures, the

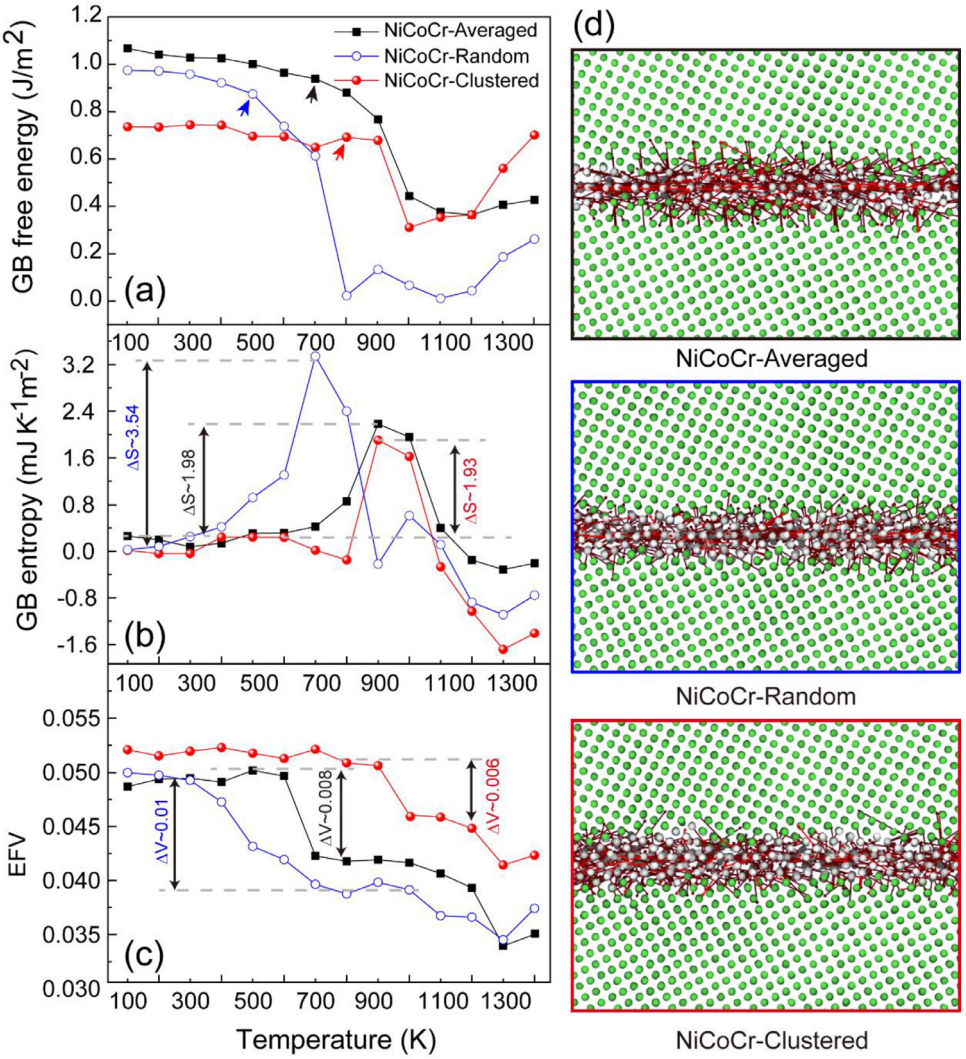

Fig. 5. The variation of GB excess properties as a function of temperature (a) excess GB free energy (b) GB excess entropy (c) excess free volume (EFV) and (d) the displacement vector of the three structures after GB transformation. The phase transition initiation temperature are marked by arrows in (a)

change of free energy is still continuous but the first derivative of free energy is discontinuity, conforms to the characteristics of first-order phase transition [7]. Furthermore, the observed discontinues points of free energy are corresponding to the maximum entropy (shown in Fig. 5b) which indicates the completion of transforms or at least an overwhelming occupation of the new Fill Kites structure. For the above reasons, we speculate that the observed discontinues changes in free energy were related to the transformation completion rather than phase transition initiation. Noting that the free energies calculated here are actually Helmholtz free energy, which is only relevant to elemental systems. In these complex multicomponent systems, the segregation of different components may affect the GB free energy, which is difficult to quantify that contribution. It should be pointed out that the element distributions are fixed for each GB configuration during free energy calculation, in which the segregation should be restrained. Moreover, for the hypothetical pure element NiCoCr-Averaged GB, the GB free energy shows a similar tendency with the multicomponent NiCoCr-Random and NiCoCr-Clustered GBs. This suggests that the other contributions to the GB free energy which stem from the segregation of different components cannot lead to a fundamentally change in the variation tendency of free energy with temperature. Therefore, the calculated Helmholtz free energy of these multicomponent GBs may still be considered reasonable.

The abrupt decrease in free energy suggests that entropic effect prevails during GB phase transformation. As shown in Fig. 5b, the GB entropy increases rapidly at the outset of transformation and then falls sharply after the GB ultimately transforms. Different from the hypothetical pure element NiCoCr-Averaged GB which only shows weak entropy fluctuation with temperature before transition point, the entropy in NiCoCr-Random GB begins increasing much earlier. This also differs from the ordered NiCoCr-Clustered GB which also exhibits a small entropy variation before transition point, suggesting that the highly disordered atom distribution with severe interatomic distortion in NiCoCr-Random GB is more unstable, needing higher entropy to compensate for the temperature induced internal energy increase. Fig. 5c shows the variation of excess free volume (EFV) with increasing temperature, in which the EFV was defined as $(V_{atom}^{GB} - V_{atom}^{Bulk})/V_{atom}^{Bulk}$, where V_{atom}^{GB} and V_{atom}^{Bulk} are the average atomic volume in GB and bulk, respectively. All the EFVs remain relatively constant at first and then decrease rapidly when the phase transformation begins. This implies that the GB phase transformation is associated with a reduction in specific volume, which seems abnormal because the phase tran-

sition occurs at high temperature and the system should favor a less-closely-packed structure. The shrinkage of EFV highlights a reduction of excess space occupied by GB atoms, which is a result of GB structural rearrangement rather than temperature dependent lattice change. Further heating to GB pre-melting temperature did not result in another significant shrinkage of EFV, instead it rose slightly. A similar phenomenon was also found in several Ni GBs [62]. A comparison of the variation trend of EFV and GB entropy suggests that the EFV is a reflection of the relative structural distortion, which determines GB energy.

Recall that the clustering behavior of principal elements is closely related to structural distortion. The GB phase transition is thus expected to result in a drastic change in element distribution, as the structural transition caused distortion reduction, which may be one possible reason for the observation that the GB composition becomes stable at high simulation temperatures (>800 K). The obvious reduction of free energy and EFVs form Normal Kites phase to Fill-Kites phase suggests that the GB phase transformation is beneficial to bridge the gap structurally and energetically between the bulk and the GB region at intermediate temperatures. Further heating would lead to the pre-melting of GBs that increases the free energy.

Fig. 4a–c also displays a corresponding difference in the transition temperature between these GB configurations. The transition temperature was 600 K, 700 K and 1000 K for NiCoCr-Random, NiCoCr-Averaged and NiCoCr-Clustered GB configuration, respectively. According to the classical Clausius–Clapeyron equation [18] of $\frac{dp}{dT} = \frac{\Delta s}{\Delta v}$, in which p, T, Δs, Δv are pressure, temperature, entropy and volume change during phase transformation, the transition temperature depends on the entropy and volume difference before and after phase transformation. Noting that the element distributions are fixed for each GB configuration during these simulations. In this case, the changes of chemical potential and chemistry with temperature would play an unessential role in their thermodynamic arguments such as GB entropy and GB excess free volume, because it only involves the changes in relative atomic position but without element exchange. Therefore, we believe that the well-known Clausius–Clapeyron relation at least can be used for qualitative analysis of the observed GB structural transformation behaviors. According to the definition of EFV, the EFV difference between Normal Kites and Filled-Kites phase can actually be regarded as Δv. Comparing the Δs and Δv in NiCoCr-Averaged and NiCoCr-Clustered GBs shows a negligible difference of Δs and Δv which would not cause a significant difference in phase transformation temperature. Instead, Δs in NiCoCr-Random GB is ~1.8 times others, despite the similar Δv among them, which results in a lower transition temperature consistent with the results shown in Fig. 3. However, the small gap of both Δs and Δv between clustered NiCoCr-Clustered and NiCoCr-Averaged configurations is not enough to cause the significant transition temperature difference between them. Therefore, it would be reasonable to take the kinetic factor into account. Indeed, the atomic displacement in GB regions shown in Fig. 5c suggests that the GB structure transition from Normal Kites to Filled Kites is mediated by GB atomic diffusion, which is in line with other fcc metals [9].

The results of the diffusion calculations are shown in the Arrhenius diagram, Fig. 6, where the activation energies are denoted by the Q value. The first notable feature of these Arrhenius plots is the characteristic break in the slope at the demonstrated GB phase transition temperatures, signifying an abrupt change in the diffusion activation energy and providing another proof for the GB structural transition. The larger gap (~4 times) of activation energies between the low temperature Normal Kites structure and the high temperature Fill Kites structure for NiCoCr-Averaged GB is similar to the same GB in pure Cu [82], fitting the pure element character of our NiCoCr-Averaged sample. Unexpectedly, the

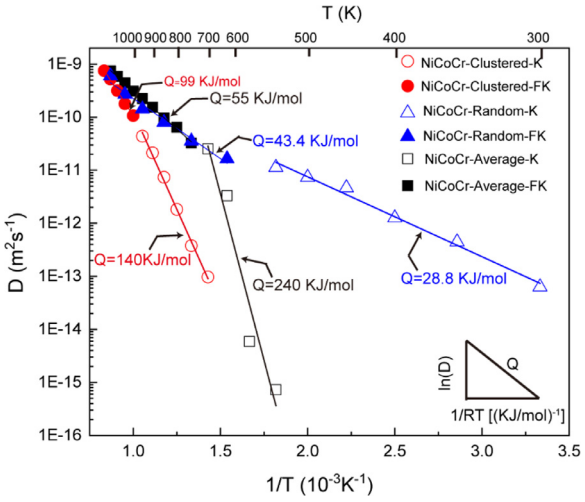

Fig. 6. Arrhenius diagram of the diffusion coefficient (D) calculated for three structures of the Σ5 (210) GB including NiCoCr-Averaged GB, NiCoCr-Random GB and NiCoCr-Clustered GB.

activation energy of Normal Kites structure in NiCoCr-Random GB is much lower than other more ordered GBs, contradicting to the "sluggish diffusion" effect deuced from its high configuration entropy [83,84]. By using the radiotracer analysis, Vaidya et al. also observed a non-sluggish diffusion behavior of GB in CoCrFeMnNi HEA when the constituent diffusivities were compared with other FCC alloys [85,86]. These results substantiate the fact that an increased configurational entropy cannot a priori be considered as the sufficient condition for diffusion being sluggish [87–89], at least in GB. The low activation energies and high diffusion coefficient of NiCoCr-Random GB suggest that the atoms within random GB are more liable to move, which leads to the lowest phase transition temperature. Note that the activation energy of NiCoCr-Averaged Kites GB (NiCoCr-Averaged-K) is higher than that of NiCoCr-Clustered GB, seemingly contradicting its lower transition temperature. One possible reason for this discrepancy may be related to the larger difference in free energy that provides stronger transition driving force thermodynamically for NiCoCr-Averaged GB.

The calculated diffusion activation energy for ordered NiCoCr-Clustered GB is 140 KJ/mol at low temperature regime (<1000 K), which is comparable to the recent experimental result for a CoCrFeMnNi HEA where the activation energy of constituting elements is ~180 KJ/mol [86]. This is expected since the tested sample has been homogenized at 1373 K for 50 h before diffusion measurement, in which the heterogeneously segregation or local chemical order will be formed [28,51,86]. The significant gap in the diffusion behavior between NiCoCr-Clustered and NiCoCr-Random GB suggests that the microscopic degrees of freedom such as LCO or compositional modulation plays a crucial role in the GB diffusion, precipitation or phase transition behaviors. This could be another reason, besides the observed phase decomposition, for the appearance of the two distinct branches observed in the penetration profile during experimental diffusion measurements in the NiCoCrFeMn HEA [86] and Ni–Cr–Fe alloy [31]. Whereas the impact of compositional modulation and phase decomposition on the observed diffusion branches might be complex and not straightforward, since it is challenging to clearly judge what mechanism decided the enhanced atomic transport in experiment. The change of compositional modulation (or LCO) to phase decomposition is actually a continuous process. For example, Li et al. believe that GB compositional modulation (local ordered clusters) in HEAs can serve as spinodal precursor states for phase nucleation which promote

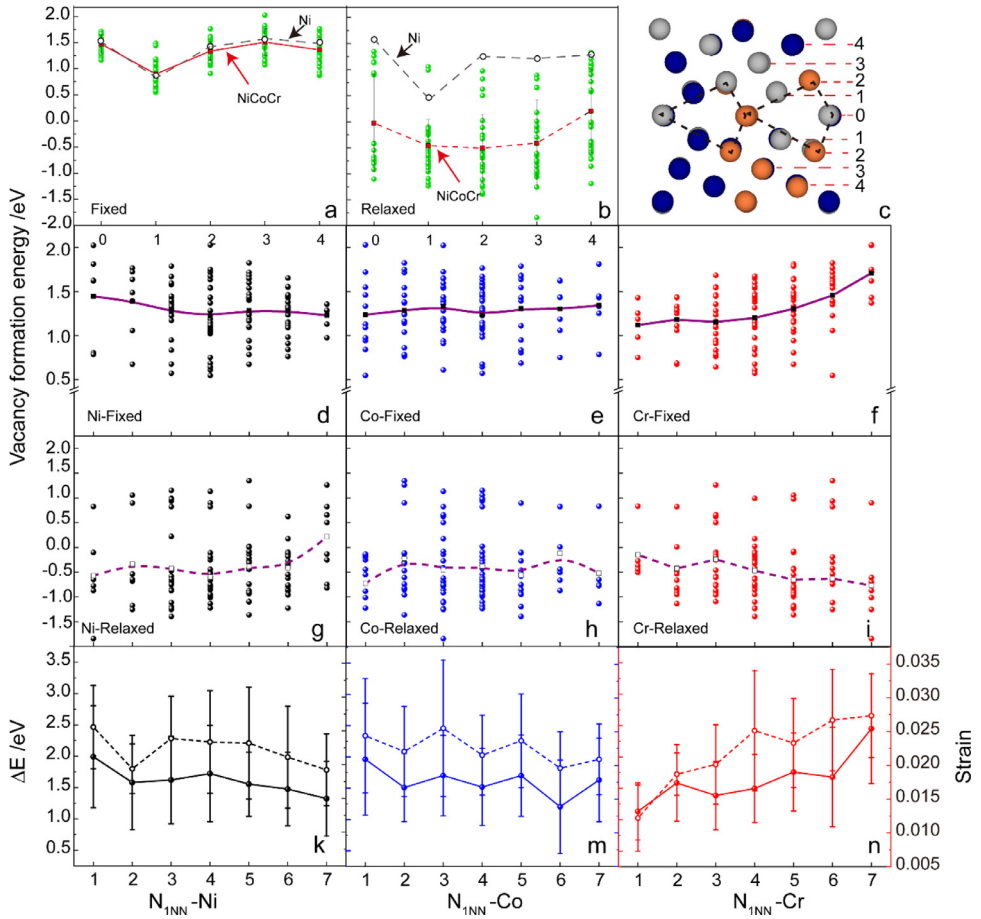

Fig. 7. Dependence of vacancy formation energies (VFEs) on their atomic environments: (a–c) VEFs as function of distance away from the GB plane calculated (a) without and (b) with atom relaxation, and (c) corresponding GB model; (d–f) the variation of VFEs with the number of (d) Ni (e) Co and (f) Cr within a radius of 3 Å around vacancies calculated without atom relaxation; (g–i) he variation of VFEs with the number of (d) Ni (e) Co and (f) Cr within a radius of 3 Å around vacancies calculated with full atom relaxation; (k–n) dependency of the structure relaxation induced reduction of EFV (left, solid line, ΔE) and corresponding atomic strain (right, dash line) to the number of (k) Ni (m) Co and (n) Cr within a radius of 3 Å around vacancies.

interfacial phase-like transitions or precipitation [28]. Nevertheless, our simulations substantiate that GB segregation and chemical ordering plays an important role in GB diffusion which serves as the kinetics factor for structural transformation.

3.3. Vacancy mechanism for GB diffusion and transformation

Understanding the formation and migration behaviors of point defects is crucial to explore the diffusion and thus phase transformation behavior in these CCA GBs [90]. In this study, we only consider vacancy behaviors as a representative. To give a more detailed and accurate description of GB defect behaviors, we first employ DFT to calculate the vacancy formation energy (VFE) in Σ5 (210) STGB of NiCoCr alloy and the results are shown in Fig. 7.

Fig. 7a and b show the VFEs as function of the distance away from the GB plane (0 layer, marked in Fig. 7c) calculated with (Fixed, shown in Fig. 7a) and without (Relaxed, Fig. 7b) atom relaxation, and corresponding values for pure Ni also plotted for comparison. If we only consider the chemical effect on vacancy formation, as shown in Fig. 7a, the trend of the average VFEs is the same as that of pure Ni, i.e., L1 layer possesses the lowest VFE due to the large compressive stress. In this situation, the EFVs in the CCA GB are positive and their average values are comparable with pure Ni. But when the atoms are fully relaxed, the majority of VEFs decreased dramatically to negative for CCA GB, contrary to the minor reduction in the case of pure Ni. This reflects the vital role of local structure distortion on the formation of vacancy for CCA. In this scenario, the differential of VEFs in different GB layers is diminished, suggesting that the effect of interatomic local distortion overpowers the interplanar structural difference. Furthermore, the variations of VEF from site to site within the GB are tremendous, ranging from −2 eV to 1.5 eV, which can be linked to the existence of alternating regions of tension and compression within GB that are caused by the complex interatomic local distortion.

To investigate the effects of the local chemical environment on the VFE, we systematically analyzed the dependence of the VFEs on the number of elements within a radius of 3 Å around vacancies, as provided in Fig. 7(d–i). The static calculation results reveal that VFE is positively and negatively correlated with the number of surrounding Cr and Ni atoms, respectively, suggesting that vacancies prefer Ni-rich and Cr-poor environments (see Fig. 7d–f) when considering chemical effect only. This trend is similar to the VFEs in bulk of NiCoCr CCA after full relaxation reported previously which attributed this local chemical dependency to the effect of local electronic interaction [72,91]. However, if we take the structural relaxation into account during the calculation of GB VFEs, the reverse takes over, i.e., vacancies prefer Cr-rich as well as Ni-poor environments (see Fig. 7g–i). Fig. 7k–n exhibits the dependency of the structure relaxation induced reduction of VFEs (left, solid line, ΔE) and corresponding atomic strain (right, dash line) on the local chemical environment. Overall, structure relaxation leads to a substantial decrease in VFE, as denoted by the high

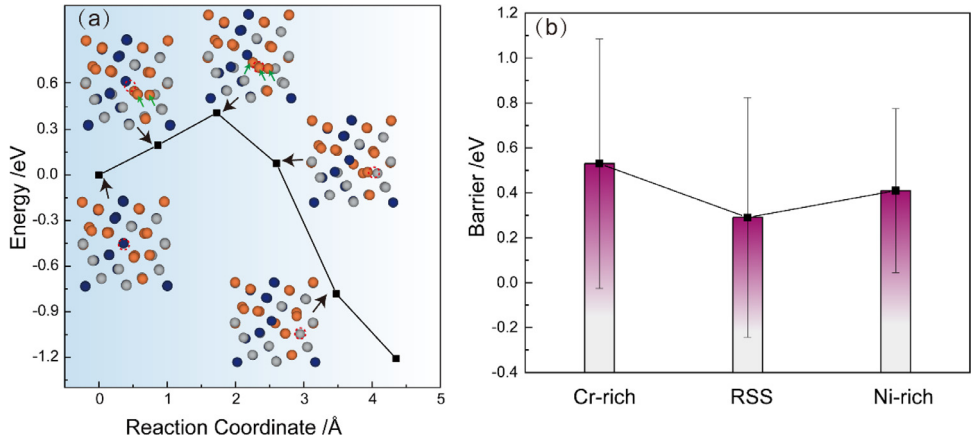

Fig. 8. Energy and pathway for the migration of vacancies: (a) representative vacancy migration pathway calculated by CI-NEB (b) Migration energy barriers vs. their chemical environment.

ΔE (~1–3 eV). These results strongly imply that the VFE in CCA GB mainly depends on local interatomic distortion rather than local electronic interaction and interplanar structural differentiation. Furthermore, the variation trend of ΔE with local chemical environment is found similar to atomic strain. The formation of vacancies in the sites with severe local distortion can release more strain energy and sometimes stabilize the GB. As demonstrated in Fig. 1d, Cr containing chemical bonds (Cr–Cr, Cr–Co or Cr–Ni) exhibit larger FWHM, implying more drastic distortion. Therefore, the more Cr atoms around the vacancies result in more local strain energy, which in turn facilitates vacancy formation to decrease system energy (Fig. 7n). In the Ni-rich chemical environment, the reverse applies. It appears reasonable to assume that the NiCoCr-Clustered GB shown in Fig. 3c and d would generate less vacancies at low temperature (before phase transition) due to its pronounced Ni–Ni clustering.

The self-diffusion activation energy on the basis of a vacancy exchange model can be expressed as the sum of the vacancy formation and migration energy [92]. We thus further calculated the vacancy migration barriers in GB by using CI-NEB to evaluate the dependency of vacancy migration energy on their local chemical environment. The results are shown in Fig. 8. Fig. 8a shows a representative vacancy migration pathway. As seen, the movement of vacancy is not by direct exchanging with individual atom but by the simultaneous motion of two atoms (marked by green arrows), coinciding with the so called “long vacancy jumps” that arise from the existence of unstable vacancies [90]. These unstable vacancies are related to the vacancy delocalization induced by the drastic structure relaxations around vacancy [93], which would be more abundant in the Cr-rich regions (see Fig. 7n) due to its severe distortion. Fig. 8b shows the migration energy barriers vs. their chemical environment, in which only Ni-rich environment (N_{1nn}-Ni > 5), random environment and Cr-rich environment (N_{1nn}-Ni > 5) are considered. Overall, the magnitude of the vacancy migration barrier follows the sequence of random < Ni-rich environment < Cr-rich environment. In general, the migration barriers are determined by the energy difference between the saddle and initial states. For random environment, the structure perturbation and thus energy change caused by atom movement could be smaller than more ordered environments such as Ni-rich and Cr-rich environments, corresponding to the lowest vacancy migration barrier in the random environment. Similarly, it has been reported that the vacancy migration barriers in random NiCoCr and NiCoFeCr CCAs are generally lower than those in pure Ni [91]. Due to the localized, directional bonding between Cr atoms [76] and its severe interatomic distortion within more ordered Cr-rich region, the movement of Cr atoms form their stable sites to saddle sites would give rise to more structural disturbance to cause an increase in energy and hence a higher migration energy.

Figs. 6–8 suggest that the GB diffusion and thus transition strongly depend on the LCO, which is manifested by the effects of local chemical environment on the formation and migration of vacancies. It is interesting to investigate to what extent the vacancy configuration controls the GB diffusion and transition. Although the Kinetic Monte Carlo (KMC) simulations allowed accurate calculations of diffusion coefficients within the GB, their results are only valid when diffusion occurs by the motion of single point defects [90]. For this reason, we calculate the diffusion directly from MD simulations, in which various GB configurations with different local environment and different number of vacancies are considered.

Based on the VFEs calculated by DFT shown in Fig. 7, it is expected that pure MC simulation that only included the chemical effects would result in a Ni-rich vacancy environment, and hybrid MCMD simulation considering both chemical and structure effects would create a Cr-rich vacancy environment. We first remove a certain number of atoms (1%, 3% and 5%) randomly from the clustered GB configuration shown in Fig. 3c, and then employ pure MC and hybrid MCMD schemes to obtain different vacancy configurations at 100 K to obtain near equiatomic GB configurations. The vacancy concentration is defined by the ratio of vacancy to the total atoms contained in the GB core which is characterized by the “Normal kites” with a width of ~0.5 nm. We pick 1%, 3% and 5% as representative of moderate vacancy concentration, for which can keep the original GB complexion [20] and roughly correspond to the GB energy minima and maximum in the plot of GB energies versus vacancy density [94]. We further investigated the GB structures with the vacancy concentration of 10–50%, the results shown that when the vacancy concentration is higher than 10%, the initial order Normal kite structure (0 K) becomes disrupted and changed to a cluttered “cyclic structure” early at a low temperature of 100 K. Further increase in temperature resulted in a similar cluttered “cyclic structure” with the absence of distinct structure transformation until eventually pre-melting at 1200 K (see Fig.S1 in the Supplemental Materials).

Fig. 9a–c shows the atom distribution around vacancies (3% vacancies) derived from the MC and hybrid MCMD simulation as well as the random GB atomic configuration that underwent equivalent anneal. As seen, the vacancies are surrounded primarily by Ni atoms for the MC simulated structure and by Cr atoms for MCMD simulated structures. These results are consistent with the DFT calculated VFEs and provide more statistical evidence that vacancies

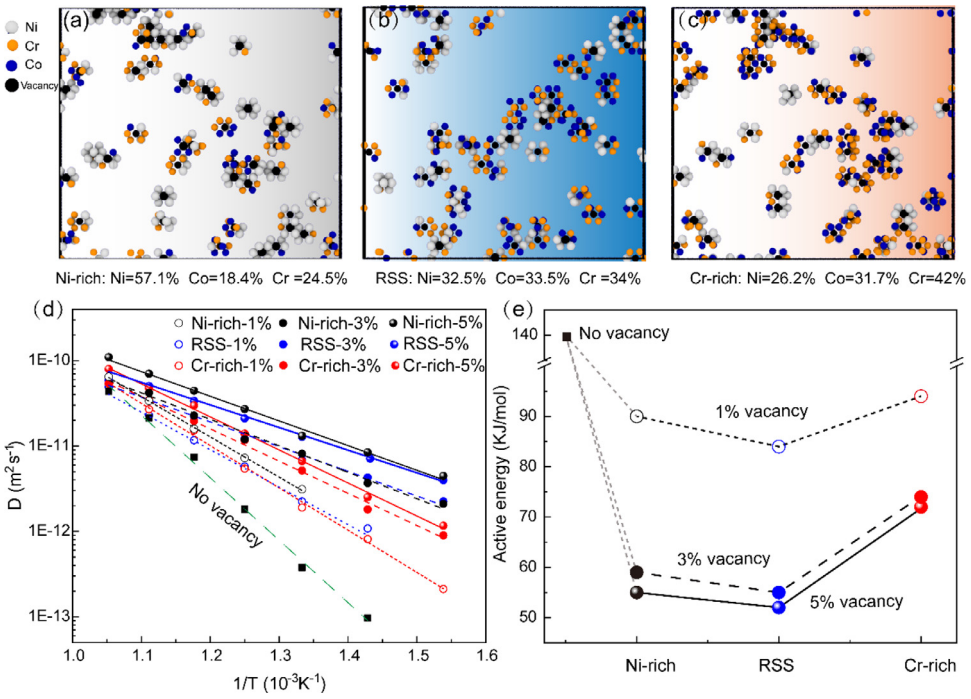

Fig. 9. Effect of vacancy configuration on GB diffusion: (a–c) GB vacancy configurations with different local environment (a) Ni-rich (b) random and (c) Cr-rich; Atoms colored by white, blue, orange and black represent Ni, Co, Cr and vacancy respectively (d) Arrhenius diagram of the diffusion coefficients for different configurations; (e) calculated diffusion active energy for different configurations.(For interpretation of the references to color in this figure legend, the reader is referred to the web version of this article.)

Table 1
Dependence of GB phase transition temperature on the vacancy content and the local environment inside the GB.

Vacancy-environment	Vacancy content			
	0	1%	3%	5%
RSS	1000 K	1000 K	800 K	600 K
Cr-rich	1000 K	1000 K	1000 K	1000 K
Ni-rich	1000 K	1000 K	1000 K	800 K

prefer Cr-rich and Ni-poor environments owing to the decisive effect of local distortion.

Fig. 9d plots the Arrhenius diagram of the diffusion coefficients for different atomic configurations containing 1%, 3% and 5% vacancy. Despite the complex chemical environment in the CCA GBs, leading to tremendous variations in vacancy formation and migration energy, the GB diffusion coefficients follow the Arrhenius Law quite well (Fig. 9d), suggesting that diffusion is actually dominated by one type of jump or perhaps a group of jumps with similar activation energies [90]. Obviously, the diffusivity in vacancy containing GBs is larger than that of intact GB, increasing with the vacancy content. This suggests a vacancy-promoted diffusion mechanism. From Fig. 9e one can clearly see that the activation energy decreases with increasing vacancy content, although the decline slows down when the vacancies exceeds 3%. Furthermore, the activation energy is the highest for Cr-rich configurations and the lowest for RSS configuration, well consistent with the trend shown in Fig. 8b calculated by CI-NEB.

These results indicate that vacancies in GB can facilitate the self-diffusion and thus phase transition in GB to varying degrees. Specifically, the promoting effect of vacancy on diffusion in Cr-rich environment is the weakest due to the relatively high activation energy and lower diffusivity. Inversely, the vacancy in RSS environments can accelerate diffusion to a great extent. Table 1 lists the effect of vacancy content and local environment on the phase transition temperature. As shown, the GBs with RSS and Ni-rich vacancy environment show decreasing transition temperature when containing 3% and 5% vacancies. In comparison, there is no significant decrease in transition temperature for the Cr-rich vacancy environment. These results are in agreement with the difference between their diffusion properties.

Now, we return to the question of how the LCO affects the GB complexion transition. Foregoing discussions demonstrate that the GB phase transition is actually controlled by vacancy assisted atomic diffusion [90]. DFT based calculations indicate that GB vacancies prefer Cr-rich as well as Ni-poor environments. Compared to RSS GB configuration, the Ni-clustering and the Co–Cr ordering GB possess more Ni-rich environments where vacancies are more difficult to be produced, indicating a sluggish diffusion behavior in the Ni-rich region. Note that some atoms in the Co–Cr ordering region possess a Cr-rich environment rather than an RSS environment. The direct diffusion simulations (Fig. 9) indicate that vacancies in Cr-rich environment are actually difficult to diffuse. Therefore, although Cr-rich environment creates vacancies easily, these vacancies can only promote diffusion to a lesser extent when compared with the RSS and even Ni-rich environment. Taking all the information gathered, the Ni-clustering and Co–Cr ordering NiCoCr CCA GBs tend to exhibit sluggish diffusion and thus a delayed phase transformation, relative to that in RSS GB.

4. Conclusion

We have studied the partition/distribution of constituent elements and structural transformation behavior in the GBs of a complex concentrated CrCoNi, taking Σ5 (210) STGB as a representative. The following conclusions can be drawn from this work:

(1) GB energy is a consequence of the competition between chemical effect and structure effect. Increasing Ni–Ni pairs can increase the GB energy due to chemical effect but decrease the GB energy due to smaller lattice distortion. Aggra-

vated structure distortion would lead to a conspicuous clustering or segregation of Ni.

(2) Similar to other fcc metals, there also exists a distinct GB structural transformation in the NiCoCr CCA. The transition temperature depends on the GB configuration. The CCA GB with random atomic distribution is more conducive to transformation due to larger energetic driving force and more rapid diffusion compared to a hypothetical pure A-atom alloy which bears the same bulk properties but no distinction of different elements. The transition in CCA GB can be delayed significantly, in the presence of Ni-clustering and Co–Cr ordering configurations in the GB.

(3) Cr-rich and Ni-poor environments are less conducive to the formation of GB vacancies, suggesting that a Ni-clustered GB structure would make it more difficult to generate vacancies to mediate GB diffusion. Moreover, the migration of vacancies in Ni-rich and Cr-rich environment are more difficult than in a random solution environment; vacancies in a random environment exhibit a lower activation barrier. Our analysis taking both factors into consideration indicates that, compared with the random NiCoCr GB, the GB containing local Ni-clustering and Co–Cr ordering exhibits more sluggish diffusion and thus a delayed GB phase transformation.

Declaration of Competing Interest

Authors declare that they have no conflict of interest.

Acknowledgments

The authors thank Dr. Qingjie Li (Massachusetts Institute of Technology) for discussions on MCMD simulation. This work is supported by the National Key Research and Development Program of China (No. 2017YFB0702003), the NSFC Basic Science Center Program for “Multi-scale Problems in Nonlinear Mechanics” (No. 11988102), the NSFC (Nos. 11790292 and 11972346), the Strategic Priority Research Program (Nos. XDB22040302 and XDB22040303), the Key Research Program of Frontier Sciences (Grant no. QYZDJSSW- JSC011), Science Challenge Project (No. TZ2016001), and the opening project of State Key Laboratory of Explosion Science and Technology. E.M. acknowledges IM-CAS for hosting his research.

Supplementary materials

Supplementary material associated with this article can be found, in the online version, at doi:10.1016/j.actamat.2021.116786.

References

[1] D. Prokoshkina, V.A. Esin, G. Wilde, S.V. Divinski, Grain boundary width, energy and self-diffusion in nickel: effect of material purity, Acta Mater. 61 (2013) 5188–5197.
[2] T. Chookajorn, H.A. Murdoch, Christopher A. Schuh, Design of stable nanocrystalline alloys, Science 337 (2012) 951–955.
[3] S.V. Divinski, G. Reglitz, G. Wilde, Grain boundary self-diffusion in polycrystalline nickel of different purity levels, Acta Mater. 58 (2010) 386–395.
[4] V. Randle, G.S. Rohrer, H.M. Miller, M. Coleman, G.T. Owen, Five-parameter grain boundary distribution of commercially grain boundary engineered nickel and copper, Acta Mater. 56 (2008) 2363–2373.
[5] J. Wang, I.J. Beyerlein, C.N. Tomé, Reactions of lattice dislocations with grain boundaries in Mg: implications on the micro scale from atomic-scale calculations, Int. J. Plasticity 56 (2014) 156–172.
[6] M. Chassagne, M. Legros, D. Rodney, Atomic-scale simulation of screw dislocation/coherent twin boundary interaction in Al, Au, Cu and Ni, Acta Mater. 59 (2011) 1456–1463.
[7] P.R. Cantwell, M. Tang, S.J. Dillon, J. Luo, G.S. Rohrer, M.P. Harmer, Grain boundary complexions, Acta Mater. 62 (2014) 1–48.
[8] T. Meiners, T. Frolov, R.E. Rudd, G. Dehm, C.H. Liebscher, Observations of grain-boundary phase transformations in an elemental metal, Nature 579 (2020) 375–378.
[9] M. Aramfard, C. Deng, Mechanically enhanced grain boundary structural phase transformation in Cu, Acta Mater. 146 (2018) 304–313.
[10] T. Frolov, Q. Zhu, T. Oppelstrup, J. Marian, R.E. Rudd, Structures and transitions in bcc tungsten grain boundaries and their role in the absorption of point defects, Acta Mater. 159 (2018) 123–134.
[11] V. Turlo, T.J. Rupert, Grain boundary complexions and the strength of nanocrystalline metals: dislocation emission and propagation, Acta Mater. 151 (2018) 100–111.
[12] T. Frolov, S.V. Divinski, M. Asta, Y. Mishin, Effect of interface phase transformations on diffusion and segregation in high-angle grain boundaries, Phys. Rev. Lett. 110 (2013) 1–5.
[13] M. Tang, W.C. Carter, R.M. Cannon, Grain boundary transitions in binary alloys, Phys. Rev. Lett. 97 (2006) 6–9.
[14] B. Straumal, B. Baretzky, Grain boundary phase transitions and their influence on properties of polycrystals, Interface Sci. 12 (2004) 147–155.
[15] T. Frolov, Effect of interfacial structural phase transitions on the coupled motion of grain boundaries: a molecular dynamics study, Appl. Phys. Lett. 104 (2014) 1–4.
[16] P.R. Cantwell, T. Frolov, T.J. Rupert, A.R. Krause, C.J. Marvel, G.S. Rohrer, J.M. Rickman, M.P. Harmer, Grain boundary complexion transitions, Annu. Rev. Mater. Res. 50 (2020) 465–492.
[17] C. Rottman, Theory of phase transitions at internal interfaces, J. Phys. Colloq. 49 (1988) 326.
[18] E.W. Hart, Grain boundary phase transformations, in: The Nature and Behavior of Grain Boundaries (1972) 155–170.
[19] Q. Zhu, A. Samanta, B. Li, R.E. Rudd, T. Frolov, Predicting phase behavior of grain boundaries with evolutionary search and machine learning, Nat. Commun. 9 (2018) 467.
[20] T. Frolov, D.L. Olmsted, M. Asta, Y. Mishin, Structural phase transformations in metallic grain boundaries, Nat. Commun. 4 (2013) 1–5.
[21] F. Berthier, J. Creuze, R. Tétot, B. Legrand, Structural phase transition induced by interfacial segregation: a comparison between surface and grain boundary, Appl. Surf. Sci. 177 (2001) 243–251.
[22] T. Frolov, M. Asta, Y. Mishin, Segregation-induced phase transformations in grain boundaries, Phys. Rev B 92 (2015) 020103.
[23] N. Zhou, T. Hu, J. Luo, Grain boundary complexions in multicomponent alloys: challenges and opportunities, Curr. Opin. Solid State Mater. Sci. 20 (2016) 268–277.
[24] M. Wagih, C.A. Schuh, Grain boundary segregation beyond the dilute limit : separating the two contributions of site spectrality and solute interactions, Acta Mater. 199 (2020) 63–72.
[25] W. Xing, A.R. Kalidindi, D. Amram, C.A. Schuh, Solute interaction effects on grain boundary segregation in ternary alloys, Acta Mater. 161 (2018) 285–294.
[26] S. Ma, M. Asl, C. Tansarawiput, P.R. Cantwell, M. Qi, P. Harmer, J. Luo, A grain boundary phase transition in Si–Au, Scr. Mater. 66 (2012) 203–206.
[27] J. Luo, H. Cheng, K.M. Asl, C.J. Kiely, M.P. Harmer, The role of a bilayer interfacial phase on liquid metal embrittlement, Science 333 (2011) 1730–1734.
[28] L. Li, Z. Li, A. Kwiatkowski da Silva, Z. Peng, H. Zhao, B. Gault, D. Raabe, Segregation-driven grain boundary spinodal decomposition as a pathway for phase nucleation in a high-entropy alloy, Acta Mater. 178 (2019) 1–9.
[29] K. Ming, L. Li, Z. Li, X. Bi, J. Wang, Grain boundary decohesion by nanoclustering Ni and Cr separately in CrMnFeCoNi high-entropy alloys, Sci. Adv. 5 (2019) 0639.
[30] P. Sathiyamoorthi, J. Basu, S. Kashyap, K.G. Pradeep, R.S. Kottada, Thermal stability and grain boundary strengthening in ultrafine-grained CoCrFeNi high entropy alloy composite, Mater. Des. 134 (2017) 426–433.
[31] S. Rajeshwari K., S. Sankaran, K.C. Hari Kumar, H. Rösner, M. Peterlechner, V.A. Esin, S. Divinski, G. Wilde, Grain boundary diffusion and grain boundary structures of a Ni–Cr–Fe- alloy: evidences for grain boundary phase transitions, Acta Mater. 195 (2020) 501–518.
[32] Y.F. Ye, Q. Wang, J. Lu, C.T. Liu, Y. Yang, High-entropy alloy: challenges and prospects, Mater. Today 19 (2016) 349–362.
[33] J.W. Yeh, S.K. Chen, S.J. Lin, J.Y. Gan, T.S. Chin, T.T. Shun, C.H. Tsau, S.Y. Chang, Nanostructured high-entropy alloys with multiple principal elements: novel alloy design concepts and outcomes, Adv. Eng. Mater. 6 (2004) 299–303.
[34] B. Cantor, I.T.H. Chang, P. Knight, A.J.B. Vincent, Microstructural development in equiatomic multicomponent alloys, Mater. Sci. Eng. A 375–377 (2004) 213–218.
[35] E.P. George, D. Raabe, R.O. Ritchie, High-entropy alloys, Nat. Rev. Mater. 4 (2019) 515–534.
[36] D.B. Miracle, O.N. Senkov, A critical review of high entropy alloys and related concepts, Acta Mater. 122 (2017) 448–511.
[37] Y. Zhang, T.T. Zuo, Z. Tang, M.C. Gao, K.A. Dahmen, P.K. Liaw, Z.P. Lu, Microstructures and properties of high-entropy alloys, Prog. Mater. Sci. 61 (2014) 1–93.
[38] Z. Li, S. Zhao, R.O. Ritchie, M.A. Meyers, Mechanical properties of high-entropy alloys with emphasis on face-centered cubic alloys, Prog. Mater. Sci. 102 (2019) 296–345.
[39] E.P. George, W.A. Curtin, C.C. Tasan, High entropy alloys: a focused review of mechanical properties and deformation mechanisms, Acta Mater. 188 (2020) 435–474.
[40] J.P. Liu, J.X. Chen, T.W. Liu, C. Li, Y. Chen, L.H. Dai, Superior strength-ductility CoCrNi medium-entropy alloy wire, Scr. Mater. 181 (2020) 19–24.
[41] Z. Li, K.G. Pradeep, Y. Deng, D. Raabe, C.C. Tasan, Metastable high-entropy dual-phase alloys overcome the strength-ductility trade-off, Nature 534 (2016) 227–230.

[42] S. Chen, H.S. Oh, B. Gludovatz, S.J. Kim, E.S. Park, Z. Zhang, R.O. Ritchie, Q. Yu, Real-time observations of TRIP-induced ultrahigh strain hardening in a dual-phase CrMnFeCoNi high-entropy alloy, Nat. Commun. 11 (2020) 1–8.
[43] C. Niu, C.R. LaRosa, J. Miao, M.J. Mills, M. Ghazisaeidi, Magnetically-driven phase transformation strengthening in high entropy alloys, Nat. Commun 9 (2018) 1363.
[44] E. Ma, Unusual dislocation behavior in high-entropy alloys, Scr. Mater. 181 (2020) 127–133.
[45] Z. Lei, X. Liu, Y. Wu, H. Wang, S. Jiang, S. Wang, X. Hui, Y. Wu, B. Gault, P. Kontis, D. Raabe, L. Gu, Q. Zhang, H. Chen, H. Wang, J. Liu, K. An, Q. Zeng, T.G. Nieh, Z. Lu, Enhanced strength and ductility in a high-entropy alloy via ordered oxygen complexes, Nature 563 (2018) 546–550.
[46] X.F. Liu, Z.L. Tian, X.F. Zhang, H.H. Chen, T.W. Liu, Y. Chen, Y.J. Wang, L.H. Dai, Self-sharpening" tungsten high-entropy alloy, Acta Mater. 186 (2020) 257–266.
[47] Z.J. Jiang, J.Y. He, H.Y. Wang, H.S. Zhang, Z.P. Lu, L.H. Dai, Shock compression response of high entropy alloys, Mater. Res. Lett. 4 (2016) 226–232.
[48] Z. Pu, Y. Chen, L.H. Dai, Strong resistance to hydrogen embrittlement of high--entropy alloy, Mater. Sci. Eng. A 736 (2018) 156–166.
[49] Q.-J. Li, H. Sheng, E. Ma, Strengthening in multi-principal element alloys with local-chemical-order roughened dislocation pathways, Nat. Commun. 10 (2019) 3563.
[50] J. Ding, Q. Yu, M. Asta, R.O. Ritchie, Tunable stacking fault energies by tailoring local chemical order in CrCoNi medium-entropy alloys, Proc. Natl. Acad. Sci. USA 115 (2018) 8919–8924.
[51] R. Zhang, S. Zhao, J. Ding, Y. Chong, T. Jia, C. Ophus, M. Asta, R.O. Ritchie, A.M. Minor, Short-range order and its impact on the CrCoNi medium-entropy alloy, Nature 581 (2020) 283–287.
[52] F.X. Zhang, S. Zhao, K. Jin, H. Xue, G. Velisa, H. Bei, R. Huang, J.Y.P. Ko, D.C. Pagan, J.C. Neuefeind, W.J. Weber, Y. Zhang, Local structure and short-range order in a NiCoCr solid solution alloy, Phys. Rev. Lett. 118 (2017) 205501.
[53] Q. Ding, X. Fu, D. Chen, H. Bei, B. Gludovatz, J. Li, Z. Zhang, E.P. George, Q. Yu, T. Zhu, R.O. Ritchie, Real-time nanoscale observation of deformation mechanisms in CrCoNi-based medium- to high-entropy alloys at cryogenic temperatures, Mater. Today 25 (2019) 21–27.
[54] T. Yang, Y.L. Zhao, J.H. Luan, B. Han, J. Wei, J.J. Kai, C.T. Liu, Nanoparticles-strengthened high-entropy alloys for cryogenic applications showing an exceptional strength-ductility synergy, Scr. Mater. 164 (2019) 30–35.
[55] B. Gludovatz, A. Hohenwarter, K.V Thurston, H. Bei, Z. Wu, E.P. George, R.O. Ritchie, Exceptional damage-tolerance of a medium-entropy alloy CrCoNi at cryogenic temperatures, Nat. Commun. 7 (2016) 10602.
[56] B. Gludovatz, A. Hohenwarter, D. Catoor, E.H. Chang, E.P. George, R.O. Ritchie, A fracture-resistant high-entropy alloy for cryogenic applications, Science 345 (2014) 1153–1158.
[57] J. Li, H. Chen, Q. He, Q. Fang, B. Liu, C. Jiang, Y. Liu, Y. Yang, P.K. Liaw, Unveiling the atomic-scale origins of high damage tolerance of single-crystal high entropy alloys, Phys. Rev. Mater. 4 (2020).
[58] T. Hu, S. Yang, N. Zhou, Y. Zhang, J. Luo, Role of disordered bipolar complexions on the sulfur embrittlement of nickel general grain boundaries, Nat. Commun. 9 (2018) 2764.
[59] Q. Ding, Y. Zhang, X. Chen, X. Fu, D. Chen, S. Chen, L. Gu, F. Wei, H. Bei, Y. Gao, M. Wen, J. Li, Z. Zhang, T. Zhu, R.O. Ritchie, Q. Yu, Tuning element distribution, structure and properties by composition in high-entropy alloys, Nature 574 (2019) 223–227.
[60] D. Farkas, Grain boundary structure in high-entropy alloys, J. Mater. Sci. 55 (2020) 9173–9183.
[61] D. Utt, A. Stukowski, K. Albe, Grain boundary structure and mobility in high--entropy alloys: a comparative molecular dynamics study on a Σ11 symmetrical tilt grain boundary in face-centered cubic CuNiCoFe, Acta Mater. 186 (2020) 11–19.
[62] H. Sun, C.V. Singh, Temperature dependence of grain boundary excess free volume, Scr. Mater. 178 (2020) 71–76.
[63] Y.J. Wang, G.J.J. Gao, S. Ogata, Atomistic understanding of diffusion kinetics in nanocrystals from molecular dynamics simulations, Phys. Rev. B 88 (2013) 1–7.
[64] S. Plimpton, Fast parallel algorithms for short-range molecular dynamics, J. Comput. Phys. 117 (1995) 1–19.
[65] W.R. Jian, Z. Xie, S. Xu, Y. Su, X. Yao, I.J. Beyerlein, Effects of lattice distortion and chemical short-range order on the mechanisms of deformation in medium entropy alloy CoCrNi, Acta Mater. 199 (2020) 352–369.
[66] Y. Deng, C. Deng, Size and rate dependent grain boundary motion mediated by disconnection nucleation, Acta Mater. 131 (2017) 400–409.
[67] B. Sadigh, P. Erhart, A. Stukowski, A. Caro, E. Martinez, L. Zepeda-Ruiz, Scalable parallel Monte Carlo algorithm for atomistic simulations of precipitation in alloys, Phys. Rev. B 85 (2012) 184203.
[68] A. Stukowski, Visualization and analysis of atomistic simulation data with OVITO-the open visualization tool, Model. Simul. Mater. Sci. Eng. 18 (2010) 015012.
[69] G. Kresse, J. Furthmüller, Efficiency of ab-initio total energy calculations for metals and semiconductors using a plane-wave basis set, Comput. Mater. Sci. 6 (1996) 15–50.
[70] A. van de Walle, P. Tiwary, M. de Jong, D.L. Olmsted, M. Asta, A. Dick, D. Shin, Y. Wang, L.Q. Chen, Z.K. Liu, Efficient stochastic generation of special quasirandom structures, Calphad 42 (2013) 13–18.
[71] F. Cao, Y. Jiang, T. Hu, D. Yin, Correlation of grain boundary extra free volume with vacancy and solute segregation at grain boundaries: a case study for Al, Philos. Mag. 98 (2018) 464–483.
[72] H. Guan, S. Huang, J. Ding, F. Tian, Q. Xu, J. Zhao, Chemical environment and magnetic moment effects on point defect formations in CoCrNi-based concentrated solid-solution alloys, Acta Mater. 187 (2020) 122–134.
[73] G. Henkelman, B.P. Uberuaga, H. Jónsson, Climbing image nudged elastic band method for finding saddle points and minimum energy paths, J. Chem. Phys. 113 (2000) 9901–9904.
[74] J.P. Perdew, K. Burke, M. Ernzerhof, Generalized gradient approximation made simple, Phys. Rev. Lett. 77 (1996) 3865.
[75] P.E. Blöchl, Projector augmented-wave method, Phys. Rev. B 50 (1994) 17953–17979.
[76] F.-H. Cao, Y.-J. Wang, L.-H. Dai, Novel atomic-scale mechanism of incipient plasticity in a chemically complex CrCoNi medium-entropy alloy associated with inhomogeneity in local chemical environment, Acta Mater. 194 (2020) 283–294.
[77] R. Freitas, M. Asta, M. De Koning, Nonequilibrium free-energy calculation of solids using LAMMPS, Comput. Mater. Sci. 112 (2016) 333–341.
[78] G.S. Rohrer, The role of grain boundary energy in grain boundary complexion transitions, Curr. Opin. Solid State Mater. Sci. 20 (2016) 231–239.
[79] D. Scheiber, O. Renk, M. Popov, L. Romaner, Temperature dependence of surface and grain boundary energies from first principles, Phys. Rev. B 101 (2020) 1–13.
[80] S.M. Eich, G. Schmitz, Embedded-atom study of grain boundary segregation and grain boundary free energy in nanosized iron–chromium tricrystals, Acta Mater. 147 (2018) 350–364.
[81] T. Frolov, D.L. Olmsted, M. Asta, Y. Mishin, Structural phase transformations in metallic grain boundaries, Nat. Commun. 4 (2013) 1–7.
[82] K.C. Alexander, C.A. Schuh, An off-lattice kinetic Monte Carlo investigation of the kinetic properties of the Σ5(210) grain boundary in copper, Model. Simul. Mater. Sci. Eng. 27 (2019) 075005.
[83] K.Y. Tsai, M.H. Tsai, J.W. Yeh, Sluggish diffusion in Co–Cr–Fe–Mn–Ni high-entropy alloys, Acta Mater. 61 (2013) 4887–4897.
[84] S. Zhao, Y. Osetsky, Y. Zhang, Preferential diffusion in concentrated solid solution alloys: NiFe, NiCo and NiCoCr, Acta Mater. 128 (2017) 391–399.
[85] M. Vaidya, K.G. Pradeep, B.S. Murty, G. Wilde, S.V. Divinski, Radioactive isotopes reveal a non sluggish kinetics of grain boundary diffusion in high entropy alloys, Sci. Rep. 7 (2017) 1–11.
[86] M. Glienke, M. Vaidya, K. Gururaj, L. Daum, B. Tas, L. Rogal, K.G. Pradeep, S.V. Divinski, G. Wilde, Grain boundary diffusion in CoCrFeMnNi high entropy alloy: kinetic hints towards a phase decomposition, Acta Mater. 195 (2020) 304–316.
[87] M. Vaidya, G.Mohan Muralikrishna, S.V. Divinski, B.S. Murty, Experimental assessment of the thermodynamic factor for diffusion in CoCrFeNi and CoCrFeMnNi high entropy alloys, Scr. Mater. 157 (2018) 81–85.
[88] M. Vaidya, S. Trubel, B.S. Murty, G. Wilde, S.V. Divinski, Ni tracer diffusion in CoCrFeNi and CoCrFeMnNi high entropy alloys, J. Alloys Compd. 688 (2016) 994–1001.
[89] S.V. Divinski, A.V. Pokoev, N. Esakkiraja, A. Paul, A Mystery of "sluggish diffusion" in high-entropy alloys: the truth or a myth? Diffus. Found. 17 (2018) 69–104.
[90] A. Suzuki, Y. Mishin, Atomic mechanisms of grain boundary diffusion: low versus high temperatures, J. Mater. Sci. 40 (2005) 3155–3161.
[91] S. Zhao, T. Egami, G.M. Stocks, Y. Zhang, Effect of d electrons on defect properties in equiatomic NiCoCr and NiCoFeCr concentrated solid solution alloys, Phys. Rev. Mater. 2 (2018) 013602.
[92] R.W. Balluffi, Grain boundary diffusion mechanisms in metals, in: Metallurgical Transactions. A, Physical Metallurgy and Materials Science, 1982, pp. 2069–2095.
[93] A. Suzuki, Y. Mishin, Interaction of point defects with grain boundaries in fcc metals, Interface Sci. 11 (2003) 425–437.
[94] W.S. Yu, M.J. Demkowicz, Non-coherent Cu grain boundaries driven by continuous vacancy loading, J. Mater. Sci. 50 (2015) 4047–4065.